© 2017. Published by The Company of Biologists Ltd | Development (2017) 144, 2683-2693 doi:10.1242/dev.152108

RESEARCH ARTICLE

SPEF2 functions in microtubule-mediated transport in elongating spermatids to ensure proper male germ cell differentiation

Mari S. Lehti[1,2,*], Fu-Ping Zhang[2,3,*], Noora Kotaja[2,*] and Anu Sironen[1,‡,§]

ABSTRACT

Sperm differentiation requires specific protein transport for correct sperm tail formation and head shaping. A transient microtubular structure, the manchette, appears around the differentiating spermatid head and serves as a platform for protein transport to the growing tail. Sperm flagellar 2 (SPEF2) is known to be essential for sperm tail development. In this study we investigated the function of SPEF2 during spermatogenesis using a male germ cell-specific *Spef2* knockout mouse model. In addition to defects in sperm tail development, we observed a duplication of the basal body and failure in manchette migration resulting in an abnormal head shape. We identified cytoplasmic dynein 1 and GOLGA3 as novel interaction partners for SPEF2. SPEF2 and dynein 1 colocalize in the manchette and the inhibition of dynein 1 disrupts the localization of SPEF2 to the manchette. Furthermore, the transport of a known SPEF2-binding protein, IFT20, from the Golgi complex to the manchette was delayed in the absence of SPEF2. These data indicate a possible novel role of SPEF2 as a linker protein for dynein 1-mediated cargo transport along microtubules.

KEY WORDS: Spermatogenesis, Manchette, Dynein, Golgi complex, Protein transport, Intraflagellar transport 20

INTRODUCTION

Spermiogenesis is a complex process whereby haploid round spermatids undergo morphological transformation into spermatozoa. This process includes sperm head shaping, chromatin condensation, acrosome and manchette formation, sperm tail development and, finally, removal of excess cytoplasm. Sperm flagellar 2 (SPEF2; also known as KPL2) is crucial for sperm tail and cilia function (Sironen et al., 2006), but its molecular function has remained unresolved. *Spef2* is expressed in various ciliated tissues, such as the trachea, brain, kidney, lung, spleen and testis (Ostrowski et al., 1999), and it has several splicing variants with tissue-specific expression (Sironen et al., 2006, 2010). Spontaneous mutation in *Spef2* caused infertility in the Finnish Yorkshire pig population due to short and immotile sperm tails (Sironen et al., 2006). The causative mutation was established as an Line-1 sequence insertion in intron 30 of the *Spef2* gene resulting in a premature translation stop codon (Sironen et al., 2006, 2002). Mutations in the *Spef2* gene (an amino acid substitution within exon 3 and a nonsense mutation within exon 28) in the *big giant head* (*bgh*) mouse model caused a primary ciliary dyskinesia (PCD)-like phenotype, including hydrocephalus, sinusitis and male infertility (Sironen et al., 2011). Detailed analysis of spermatogenesis in both pig and mouse models revealed axonemal abnormalities, including defects in central pair (CP) structure and the complete disorganization of the sperm tail (Sironen et al., 2011). A role of SPEF2 in protein transport has been postulated owing to its known interaction and colocalization with intraflagellar transport 20 (IFT20). During spermatogenesis, IFT20 and SPEF2 colocalize in the Golgi complex of late spermatocytes and round spermatids and in the manchette and basal body of elongating spermatids (Sironen et al., 2010).

Intraflagellar transport (IFT) is known to be essential for cilia development and maintenance, and it also functions during sperm tail development. IFT employs motor proteins along the axonemal microtubular doublets to deliver proteins to the site of cilia assembly. During IFT, two motor proteins are responsible for cargo transport: kinesin 2 motors, which function in anterograde transport, and dynein 2 motors, which function in retrograde transport (Scholey, 2013; Taschner and Lorentzen, 2016). We have shown that depletion of heterotrimeric kinesin 2 subunit KIF3A in postnatal male germ cells results in severe defects in sperm tail development, suggesting that KIF3A-mediated transport operates also in the construction of the sperm flagellum (Lehti et al., 2013). Interestingly, spermatid head shaping was also affected in *Kif3a* knockout spermatids due to defective function of the manchette during elongation of the spermatid head. The manchette is a microtubule- and F-actin-containing structure that appears at step 8 of spermatid differentiation to surround the spermatid head. As well as participating in spermatid head shaping, the manchette has been shown to serve as a site for protein delivery to the growing tail via a motor protein-mediated process called intramanchette transport (IMT). IMT has been suggested to resemble IFT, and many IFT proteins have been localized to the manchette (Hayasaka et al., 2008; Kierszenbaum et al., 2011a; Lehti et al., 2013; Navolanic and Sperry, 2000; Nozawa et al., 2014; Saade et al., 2007; Sironen et al., 2010; Yoshida et al., 1994).

In addition to KIF3A, IFT88, which is a component of the kinesin 2-binding IFT complex B, has been implicated in IFT and IMT during spermiogenesis. Indeed, *Ift88* mutant mice share similar defects with *Kif3a* knockout mice (Kierszenbaum et al., 2011b). In wild-type mice, vesicles positive for the IFT88-interacting protein GMAP210 (TRIP11) were seen first in *cis*-Golgi, and then they sequentially colocalized with IFT88 in proacrosomal vesicles, acrosome membranes, the head-tail coupling apparatus and developing tail. However, in *Ift88* mutant mice, Golgi-derived GMAP210-positive vesicles did not reach the tail region, suggesting defective IMT (Kierszenbaum et al., 2011b).

In this study we have generated a male germ cell-specific conditional knockout (cKO) mouse model for *Spef2* to understand

[1]Natural Resources Institute Finland (Luke), Green Technology, FI-31600 Jokioinen, Finland. [2]Department of Physiology, Institute of Biomedicine, University of Turku, FI-20520 Turku, Finland. [3]Turku Center for Disease Modeling, University of Turku, FI-20520 Turku, Finland.
*Present address: Institute of Biomedicine, University of Turku, Kiinamyllynkatu 10, Turku FI-20520, Finland. ‡Present address: University College London, Great Ormond Street Institute of Child Health, 30 Guilford Street, London WC1N 1EH, UK.

§Author for correspondence (anu.sironen@luke.fi)

A.S., 0000-0003-2064-6960

Received 14 March 2017; Accepted 11 June 2017

Development (2017) 144, 2683-2693 doi:10.1242/dev.152108

its function during spermatogenesis. Our results reveal the crucial role of SPEF2 in sperm tail development and, interestingly, in shaping of the spermatid head. Furthermore, our results suggest that SPEF2 functions in Golgi-associated protein or vesicle transport and in timely removal of the manchette during spermiogenesis.

RESULTS

Male germ cell-specific *Spef2* cKO mouse model

We created a cKO mouse model using *Ngn3* promoter-driven Cre recombinase to delete exons 3-5 of the *Spef2* gene in early postnatal male germ cells (Fig. 1A). Mice were genotyped by PCR with a specific primer pair, yielding products of 319 bp and 393 bp for the wild-type and *Spef2* floxed alleles, respectively (Fig. 1A,B). RT-PCR demonstrated that *Spef2* exons 1-3 and 1-9 were expressed in the control (CTRL) mouse testis, whereas the primer pair detecting exons 1-3 did not produce a PCR product from the cKO (Fig. 1C). Furthermore, a shorter PCR product was detected in cKO testes with a primer pair amplifying the region from exon 1 to 9, as expected (Fig. 1C). Sequencing of the RT-PCR product revealed the absence of exons 3-5 in the cKO testis; however, no stop codon was

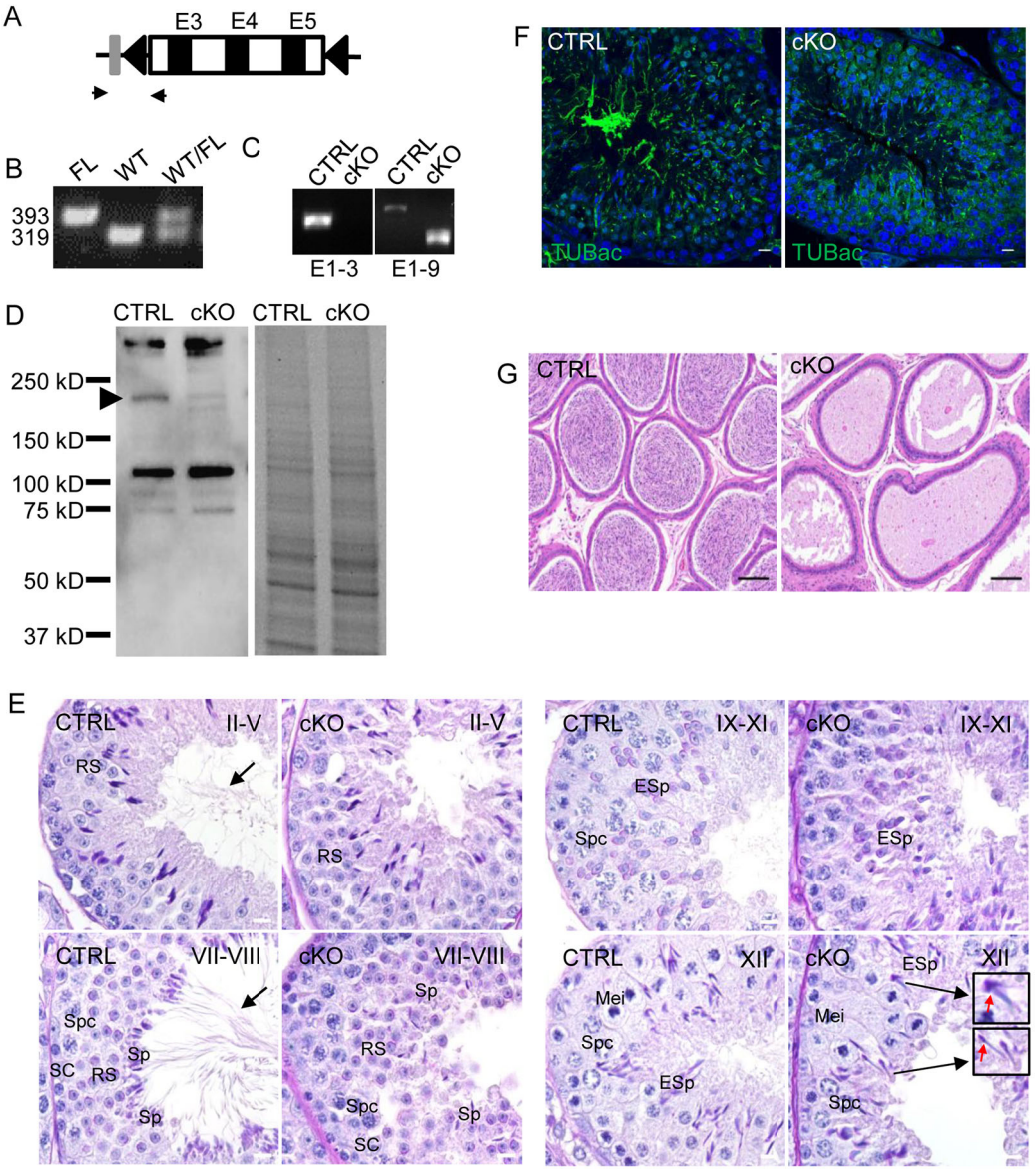

Fig. 1. The *Spef2* cKO mouse suffers from severe defects in spermatogenesis. (A) The *Spef2* cKO targeting vector contains loxP sites (arrowheads) before exon (E) 3 and after exon 5. Gray box indicates Frt site and small arrows indicate genotyping primer locations. (B) Genotyping PCR produces a 393 bp band from the *Spef2* floxed (FL) allele including the loxP site and a 319 bp band from the wild-type (WT) allele. (C) RNA was isolated from the testis of CTRL and cKO mice. RT-PCR revealed the lack of exon 3 (primers amplifying exons 1-3) and the presence of a shorter product with primers amplifying exons 1-9. (D) Western blot analysis of CTRL and cKO testis extracts showed dramatically decreased expression of the full-length SPEF2 protein (arrowhead) and the expression of truncated forms of SPEF2 in the cKO testis. Right panel illustrates equal loading of the samples as demonstrated by Coomassie Blue staining. (E) PAS staining of Bouin-fixed paraffin-embedded testis sections revealed normal spermatogenesis until haploid phase in *Spef2* cKO mice. Major differences were detected at stages II-V and VII-VIII of the seminiferous epithelial cycle, where sperm tails (arrows) were absent in the tubular lumen. At stage XII defects in elongating spermatid head shape were clearly evident in cKO testis sections (black arrows indicate the spermatids presented in the insets; red arrows show the constricted head). RS, round spermatid; Spc, spermatocyte; SC, Sertoli cell; Sp, spermatid; ESp, elongating spermatid; Mei, meiosis. (F) Absence of sperm tails was visualized using an antibody against acetylated tubulin. cKO testis sections were almost empty of acetylated tubulin signal compared with CTRL. Blue, DAPI. (G) A dramatic reduction in sperm number was apparent in HE-stained sections of the cauda epididymis of cKO mice. Scale bars: 100 µm.

Development (2017) 144, 2683-2693 doi:10.1242/dev.152108

introduced in the *Spef2* reading frame (data not shown). This suggests that a shorter SPEF2 protein product lacking the regions encoded by exons 3-5 might be expressed in the cKO testis. Indeed, western blot analysis revealed lower molecular weight SPEF2 bands in the cKO testis extract (Fig. 1D). Nonetheless, expression of the full-length SPEF2 protein (200 kDa; Spef2-002, ENSMUST00000160236, www.ensembl.org) was dramatically decreased in the cKO testis (Fig. 1D).

A functional SPEF2 N-terminus is required for correct manchette function and sperm tail formation

Depletion of *Spef2* exons 3-5 caused male infertility and the examination of testis histology revealed defective spermatogenesis. The overall organization of the seminiferous epithelium appeared normal, and no abnormalities were observed in proliferating spermatogonia or meiotic spermatocytes. However, the late steps of haploid differentiation were severely compromised. The most prominent defects were detected in step 11-12 spermatids at stages XI and XII, where an abnormally elongated and constricted head shape was identified (Fig. 1E). In stage II-V and VII-VIII tubules containing step 13-16 spermatids, sperm tails were not detected in the tubular lumen (Fig. 1E,F). Transverse sections of the cKO cauda epididymis demonstrated dramatic reduction in the amount of sperm; hardly any spermatozoa were seen in the cauda tubules compared with the CTRL mouse cauda, which was filled with spermatozoa (Fig. 1G).

Phase contrast microscopy revealed clear defects in the formation of the sperm flagellum. Short and thick tails were detected at the beginning of spermatid elongation (step 9) in the cKO, as compared with the long and thin tails found in CTRL mice (Fig. 2A). The tail

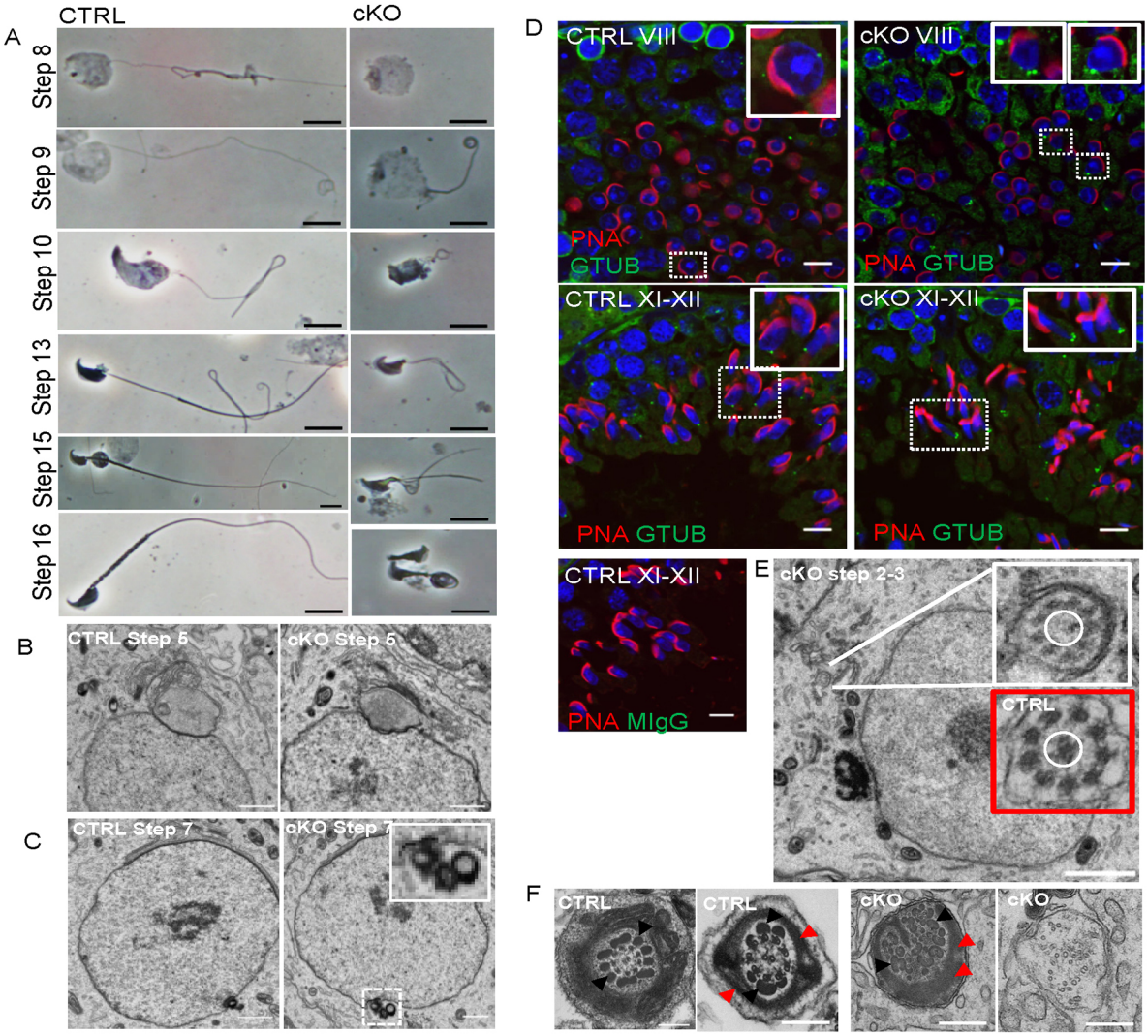

Fig. 2. Sperm tail formation is disrupted in the cKO mouse. (A) Drying-down preparations and phase contrast microscopy revealed short tails in cKO spermatids. Head defects were first seen in step 10 spermatids, where the head was detected as a cylindrical shape before its constricted form observed at later steps. Tail accessory structures were not observed in cKO mice and some spermatids appeared to have two tails or no tails. CTRL preparation showed normal sperm tail formation, assembly of principal piece and midpiece and head shaping. (B) Golgi and acrosome formation in the cKO appeared similar to that of CTRL mice. (C) In CTRL mice at step 7, a pair of centrioles was anchored to the nucleus. However, in cKO two pairs of centrioles were detected (inset). (D) γ-tubulin (green) stains the basal body, which appeared duplicated in cKO mice. PNA (red) stains the acrosome and DAPI (blue) the nucleus. MIgG, mouse immunoglobulin G. (E) At the beginning of spermiogenesis in step 2-3 spermatids the nine axonemal doublet microtubules were found correctly assembled in cKO electron microscopy preparations, but the CP of microtubules (circled) was missing. A CTRL axoneme is presented for comparison (red box insert). (F) Sperm tail structures were totally disorganized at later steps of spermiogenesis in the cKO. Black arrowheads indicate outer dense fibers (ODFs), red arrowheads indicate fibrous sheath (FS). Scale bars: 10 µm in A,D; 1 µm in B,C,E; 250 nm in F.

Development (2017) 144, 2683-2693 doi:10.1242/dev.152108

was short and malformed (bent or curved) at all steps of spermatid elongation, and in later steps 15-16 some spermatids contained two tails or no tails. Electron microscopy analysis showed that the Golgi complex and acrosome formation appeared normal (Fig. 2B,C). Interestingly, we detected a duplication of the basal body in round spermatids at step 7 (Fig. 2C). It appears that one pair of centrioles was attached to the other pair of centrioles (Fig. 2C), but only one implantation fossa was present on the nuclear surface. The basal body duplication was confirmed by immunostaining with an antibody against γ-tubulin (Fig. 2D).

Correlating with the prominent defects in tail formation detected by light microscopy, the CP of the axonemal microtubules was missing in the cKO round spermatids (Fig. 2E). In addition to the axoneme formation, the assembly of sperm tail accessory structures was also defective. No mitochondrial sheath or fibrous sheath (FS) formation was detected in cKO spermatids, as demonstrated by flagella that were thin in appearance in phase contrast microscopy (Fig. 2A). Electron microscopy showed that components required for the construction of the FS and outer dense fibers (ODFs) were present but mislocalized in cKO spermatids (Fig. 2F).

The abnormal head shape appears to arise from compromised manchette function. In the cKO mice, manchette microtubules were assembled along the nucleus similar to CTRL mice (Fig. 3A). However, they appeared abnormally long and to constrict the head starting from step 11-12, when the manchette should start moving towards the sperm tail (Fig. 3A,B). Immunofluorescent staining with α-tubulin antibody confirmed the defect in manchette clearance (Fig. 3C). Abnormally long manchettes were frequently detected in step13-14 spermatids during stages I-II, whereas in most of the CTRL step 13-14 spermatids the manchette had already disappeared (Fig. 3C).

The dynein 1 complex drives SPEF2 transport

Anti-SPEF2 immunoprecipitation from total testis extracts followed by mass spectrometry analysis identified several possible interaction candidates (Table 1). Interestingly, two proteins belonging to the cytoplasmic dynein 1 complex were identified as SPEF2-interacting proteins, including cytoplasmic dynein 1 heavy chain 1 (DYNC1H1) and intermediate chain 2 (DYNC1I2). We confirmed the DYNC1I2 protein interaction with SPEF2 in the CTRL testis by co-IP with DYNC1I2 antibody followed by western blot analysis with SPEF2 antibody (Fig. 4A). Furthermore, dynein was shown to localize to the manchette during spermiogenesis (Fig. 4B). We have previously shown that SPEF2 is also found in the manchette (Sironen et al., 2010), which suggests that the manchette provides a site for the functional interaction of SPEF2 and the dynein 1 complex. The manchette localization of DYNC1I2 was restricted to the area covering the nucleus, whereas manchette microtubules that were detached and extending over the connecting piece were found to be DYNC1I2 negative (Fig. 4B). In addition to the manchette, DYNC1I2 localized in the cytoplasm of pachytene spermatocytes (Fig. 4B) and round spermatids (data not shown).

The overall localization of DYNC1I2 was not affected in cKO mouse testis sections (Fig. 4B), which indicated that dynein localization is not dependent on SPEF2. We then hypothesized that dynein 1 might act as a motor protein for SPEF2 during spermiogenesis. Thus, we tested whether the inhibition of cytoplasmic dynein affects the localization of SPEF2 during spermatid elongation. We set up a seminiferous tubule culture system and incubated stage-specific (stage IX-XI) segments of seminiferous tubules in the presence of 200 µM ciliobrevin D (Firestone et al., 2012). After 3 h incubation, we observed a significant difference in SPEF2 localization compared with the DMSO-treated control (Fig. 4C,D). In control spermatids, SPEF2 was not equally distributed to the whole manchette: the staining covered the posterior half of the manchette, leaving the area closest to the perinuclear ring devoid of SPEF2 signal. By contrast, after ciliobrevin D treatment, SPEF2 staining was detected along the whole manchette, reaching also to the area adjacent to the perinuclear ring. These results indicate that dynein activity is required for the correct distribution of SPEF2 along the manchette microtubules (Fig. 4C,D).

IFT20 transport is delayed in the absence of functional SPEF2

Previously, we have identified IFT20 as an interacting partner for SPEF2 (Sironen et al., 2010). The localization patterns for IFT20 and SPEF2 are very similar during spermiogenesis. Both proteins are localized in the Golgi complex of late spermatocytes and round spermatids and in the manchette and basal body of elongating spermatids (Sironen et al., 2010). The possibility that SPEF2 has a role in protein transport from the Golgi complex and through the manchette towards the sperm tail prompted us to investigate the localization of IFT20 during spermiogenesis in the cKO mice. IFT20-specific signal was detected as a ring-shaped staining surrounding the *cis*-Golgi in late spermatocytes. However, the staining appeared more cytoplasmic in the cKO and the clear ring staining was reduced, suggesting a possible defect in concentrating IFT20 to the Golgi complex (Fig. 5A). Thus, SPEF2 function is not limited to late spermiogenesis, but it functions already in meiotic cells in Golgi-associated transport. This is further supported by the identification of Golgin subfamily A member 3 (GOLGA3), a protein with a well-characterized role in Golgi function (Yadav et al., 2012), as an interaction partner for SPEF2 (Table 1). GOLGA3 was localized to the Golgi complex in spermatocytes and round spermatids and in the acrosome/acroplaxome in round spermatids (Fig. 5B,C). GOLGA3 localization was not affected in cKO mice (Fig. 5B,C).

The distribution of the cytoplasmic IFT20 signal in step 9 elongating spermatids appeared affected in cKO mice (Fig. 6A). More careful immunofluorescence analysis using stage-specific drying-down preparations showed that control mice had prominent IFT20 signal in the manchette already in step 9 spermatids. By contrast, IFT20 was very weakly detected in the manchette of step 9 cKO spermatids (Fig. 6B,C). The intensity of the manchette-associated IFT20 staining in cKO step 9-10 elongating spermatids was one-third of that in controls (Fig. 6C). However, later in step 11-12 spermatids the IFT20 appeared in the cKO elongated manchette (Fig. 6B). We did not detect any reduction in the IFT20 total protein level of 4-week-old *Spef2* cKO testes that are enriched with manchette-containing elongating spermatids (the first round of spermatogenesis has progressed to the spermatid elongation phase at postnatal day 28), and which share a very similar cellular composition with 4-week-old control testes (Fig. 6D). Therefore, although the cytoplasmic IFT20 signal appeared weaker by immunofluorescence staining of stage IX-X testis transverse sections (Fig. 6A), this is likely to originate from a difference in subcellular localization rather than any decrease in the level of IFT20. In adult cKO testes, the amount of IFT20 protein was reduced (Fig. 6D), but this decrease most probably reflects the different cellular composition in *Spef2* cKO testes compared with control testes, including greatly reduced numbers of IFT20-expressing elongating spermatids and the lack of sperm tails. Altogether, these results indicate that SPEF2 is required for the efficient subcellular localization of IFT20 and transport through the manchette.

Development (2017) 144, 2683-2693 doi:10.1242/dev.152108

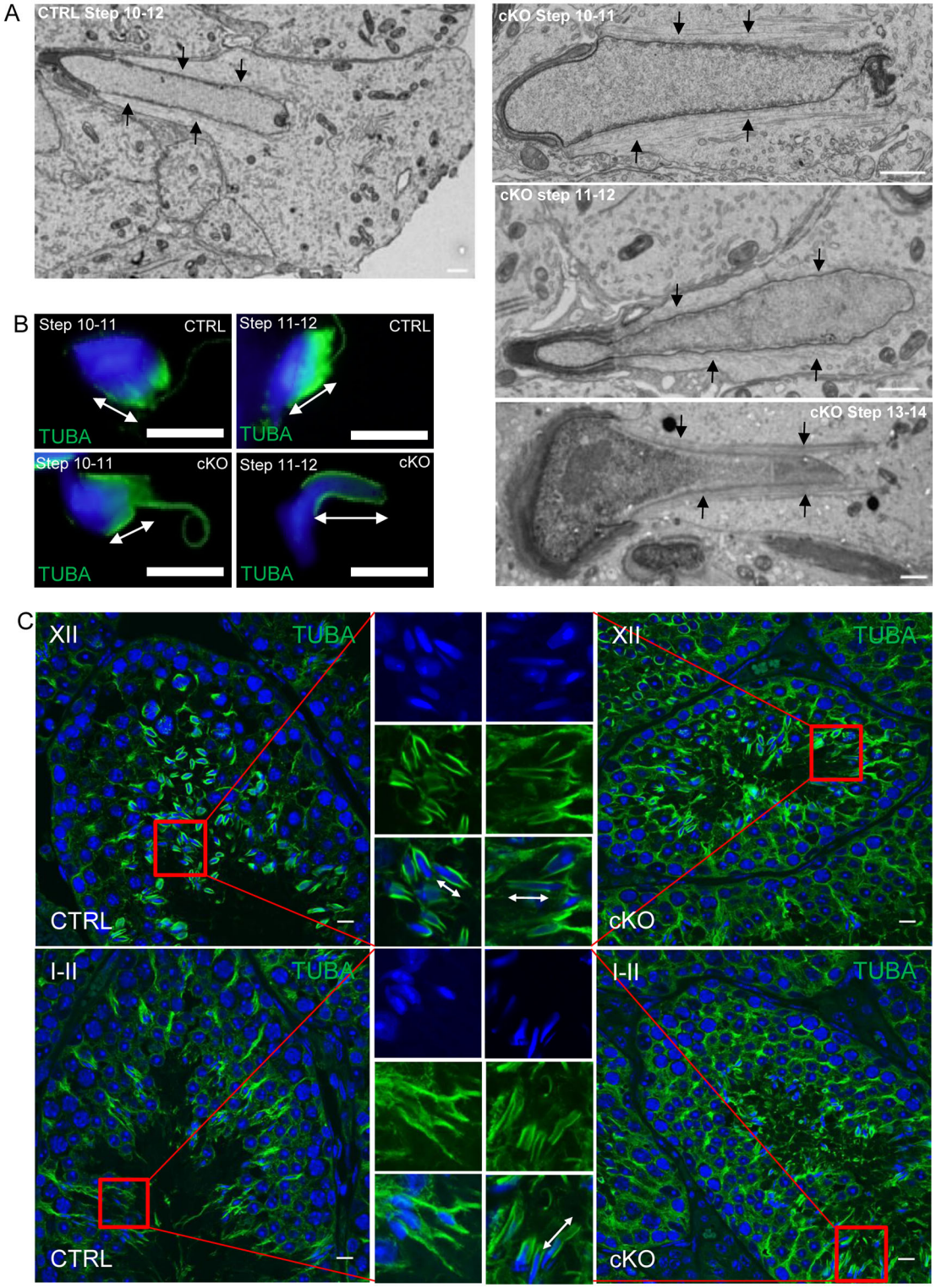

Fig. 3. Manchette clearance is delayed in the cKO mouse. (A) Electron microscopy shows correct assembly of the manchette in step 9-12 spermatids. During steps 11-12 the perinuclear ring is constricting the head, causing club-shaped head formation in the cKO. Arrows indicate manchette microtubules. (B) The manchette appeared abnormally long in step 11-12 elongating spermatids of the cKO. (C) Manchette clearance is delayed in cKO mice. During stages I-II the manchette has disappeared in the CTRL mouse, but was still present in the cKO. In B,C, α-tubulin (green) stains the manchette, DAPI (blue) stains nuclei, and double-headed arrows illustrate manchette length. Scale bars: 1 µm in A; 10 µm in B; 50 µm in C.

DISCUSSION

In this study we have demonstrated the essential role of SPEF2 in spermiogenesis and male fertility by generating a male germ cell-specific *Spef2* cKO mouse model with the deletion of exons 3-5 near the 5′ end of the gene. The cKO testis phenotype observed supports previous studies (Sironen et al., 2006, 2011, 2002) that have pointed out the important role of SPEF2 in spermatogenesis. Common features in *Spef2*-mutated pig, *bgh* and *Spef2* cKO mice are the total

Development (2017) 144, 2683-2693 doi:10.1242/dev.152108

Table 1. Identified SPEF2 interaction candidates in the mouse testis

Accession	Protein	Score	Coverage	# Unique peptides	# Peptides	# PSM
Q9JHU4	DYHC1	4810.07	22.27	119	119	138
P55937	GOLGA3	1877.05	25.35	37	37	44
O88487	DC1I2	928.48	27.29	15	18	34
Q6URW6	MYH14	916.93	8.35	3	23	25
Q8C9J3	SPEF2	906.64	12.11	22	22	23
Q62311	TAF6	779.56	30.24	18	18	22
Q7TMQ7	WDR91	706.08	21.39	15	15	15
Q569Z6	TR150	625.67	13.46	12	12	14
Q8BRT1	CLAP2	611.88	10.03	11	11	12
P50446	K2C6A	552.12	14.83	3	12	18
Q8C092	TAF5	291.91	8.24	7	7	7
P58774	TPM2	286.07	21.48	4	6	8
Q8R127	SCPDL	261.97	16.55	7	7	7
P47753	CAZA1	216.73	13.29	5	5	5
Q9ERK4	XPO2	185.66	5.46	6	6	6
Q62095	DDX3Y	183.14	6.99	2	4	4
Q8BH53	CG063	170.31	5.31	5	5	5
Q9Z2K1	K1C16	164.69	8.96	2	4	6
Q8VDM4	PSMD2	162.51	4.74	4	4	4
P62996	TRA2B	162.45	17.36	5	6	7
Q6NZA9	TAF9B	159.06	15.66	4	4	4
P13020	GELS	131.80	4.10	3	3	3
P10649	GSTM1	93.54	9.17	2	2	2
P59242	CING	87.36	2.43	3	3	3
Q8CIE6	COPA	84.13	1.63	2	2	2
Q9JJ28	FLII	72.23	1.49	2	2	2

PSM, peptide spectrum matches (total number of identified peptide sequences).

disorganization of the sperm tail and reduced number of elongating spermatids. At the beginning of spermiogenesis, axoneme elongation is initiated but fails to complete.

In addition to axonemal defects, *Spef2* cKO mice suffer from duplication of the basal body and disrupted manchette function. These additional defects compared with other *Spef2* mutant models might be a consequence of the disrupted region of SPEF2, which is shared with shorter 5′ end isoforms in addition to full-length SPEF2. Interestingly, the phenotype of *Spef2* cKO mice shares prominent similarities with *Katnb1* mutant mice, which are defective in the p80 regulatory subunit (KATNB1) of the katanin microtubule-severing complex, including abnormal elongation of the manchette and the loss of axonemal CP microtubules (O'Donnell et al., 2012). In addition to the p80 subunit, the katanin complex contains the p60 severing enzyme (KATNA1), which is involved in microtubule dynamics. Although we have not observed any direct link between katanin and SPEF2, the phenotypic similarities suggest that they might function in the same pathway. Just like SPEF2, KATNB1 has been shown to interact with cytoplasmic dynein (Jin et al., 2017). However, while we showed that SPEF2 is likely to function downstream of dynein, KATNB1 has been shown to inhibit dynein motility, suggesting that it functions as an upstream regulator of dynein. This might also explain the more prominent effects of *Katnb1* mutations (O'Donnell et al., 2012) in various tissues as compared with the more subtle and tissue-specific effects of *Spef2* depletion.

Duplication of a pair of centrioles was observed in *Spef2* cKO spermatids and this was more clearly visible when centrioles were attached to the nucleus via implantation fossa. However, the overall structure of the basal body appeared normal. Interestingly, *in vitro* studies have shown that depletion of the p80 or p60 katanin subunit also causes centriole duplication (Hu et al., 2014; Ververis et al., 2016). The mechanism via which SPEF2 or katanin is involved in centriole duplication remains unknown. Centriole duplication requires the disengagement of the centriole pair, which is important for licensing initiation of the next centriole duplication cycle (Nigg and Stearns, 2011). In *C. elegans*, it has been shown that the disengagement is inhibited by specific mechanisms during meiosis II to prevent centriole duplication, resulting in only one tightly engaged centriole pair in haploid spermatids (Schvarzstein et al., 2013). It is an interesting possibility that SPEF2 has a role in this process, and the absence of SPEF2 could result in the aberrant disengagement of the centriole pair followed by the duplication of centrioles at the final phase of meiosis. SPEF2 is known to be highly expressed in spermatocytes (Sironen et al., 2010), supporting its possible function during meiosis, although the most obvious spermatogenic defects in *Spef2* cKO mice can be detected much later in elongating spermatids.

In addition to the short and malformed sperm tail, the abnormal nuclear shape of elongating spermatids was striking in *Spef2* cKO testes. Head shaping defects appear to originate from the defective manchette function. In *Spef2* cKO mice the manchette microtubules appeared to be longitudinally assembled around the head, but at the time of manchette removal the manchette microtubules elongated abnormally and manchette removal was delayed. Interestingly, SPEF2 was shown to interact with a motor protein, the cytoplasmic dynein 1 protein complex, which transports cargos towards the minus end of microtubules. The localization of DYNC1I2 demonstrated the presence of the dynein 1 complex in the manchette. The involvement of SPEF2 in microtubule-mediated transport processes and the possible role of SPEF2 as a novel linker in dynein 1-mediated transport were further supported by the consequences of inhibition of the dynein motor, which interfered with the distribution of SPEF2 along the manchette. Although SPEF2 was not found to interact with any microtubule plus end-directed kinesins, it is interesting to note that the manchette defect in the *Spef2* cKO closely resembles the defect observed in *Kif3a* cKO spermatids (Lehti et al., 2013). Therefore, it is likely that the IMT in plus- and minus-end directions is required for the correct dynamics of manchette microtubules and IMT.

We also showed that the localization of the SPEF2 interaction partner IFT20 was affected in the *Spef2* cKO testis. Both SPEF2 and IFT20 have been localized to the Golgi complex in male germ cells (Sironen et al., 2010). In *Spef2* cKO spermatocytes IFT20 localization was still associated with the Golgi complex, but its diffuse cytoplasmic localization was greatly increased. Our results suggest that SPEF2 is required for targeting IFT20 to the Golgi complex and might be a linker protein in the microtubule-mediated transport of IFT20. Later in development, IFT20 levels were greatly reduced in the cytoplasm of early elongating spermatids, and the transport of IFT20 to the manchette was affected in *Spef2* cKO mice. Previous studies have pointed out the role of IFT20 in the intracellular transport of Golgi-derived vesicles to the ciliary base in somatic cells (Follit et al., 2006). Therefore, it is possible that a similar mechanism operates in male germ cells. This hypothesis is also supported by the confirmed interactions of SPEF2 with the dynein 1 complex and GOLGA3, which functions as a receptor in the Golgi complex membranes (Yadav et al., 2012). GOLGA3 binds dynein and this interaction is required for Golgi complex positioning and minus end-directed transport (Yadav et al., 2012). The *Golga3*^{repro27} mutant mouse model (Bentson et al., 2013) suffers from male infertility and major germ cell loss due to disrupted spermatogenesis at late meiosis. We confirmed the Golgi complex localization of GOLGA3 in male germ cells. We also

Development (2017) 144, 2683-2693 doi:10.1242/dev.152108

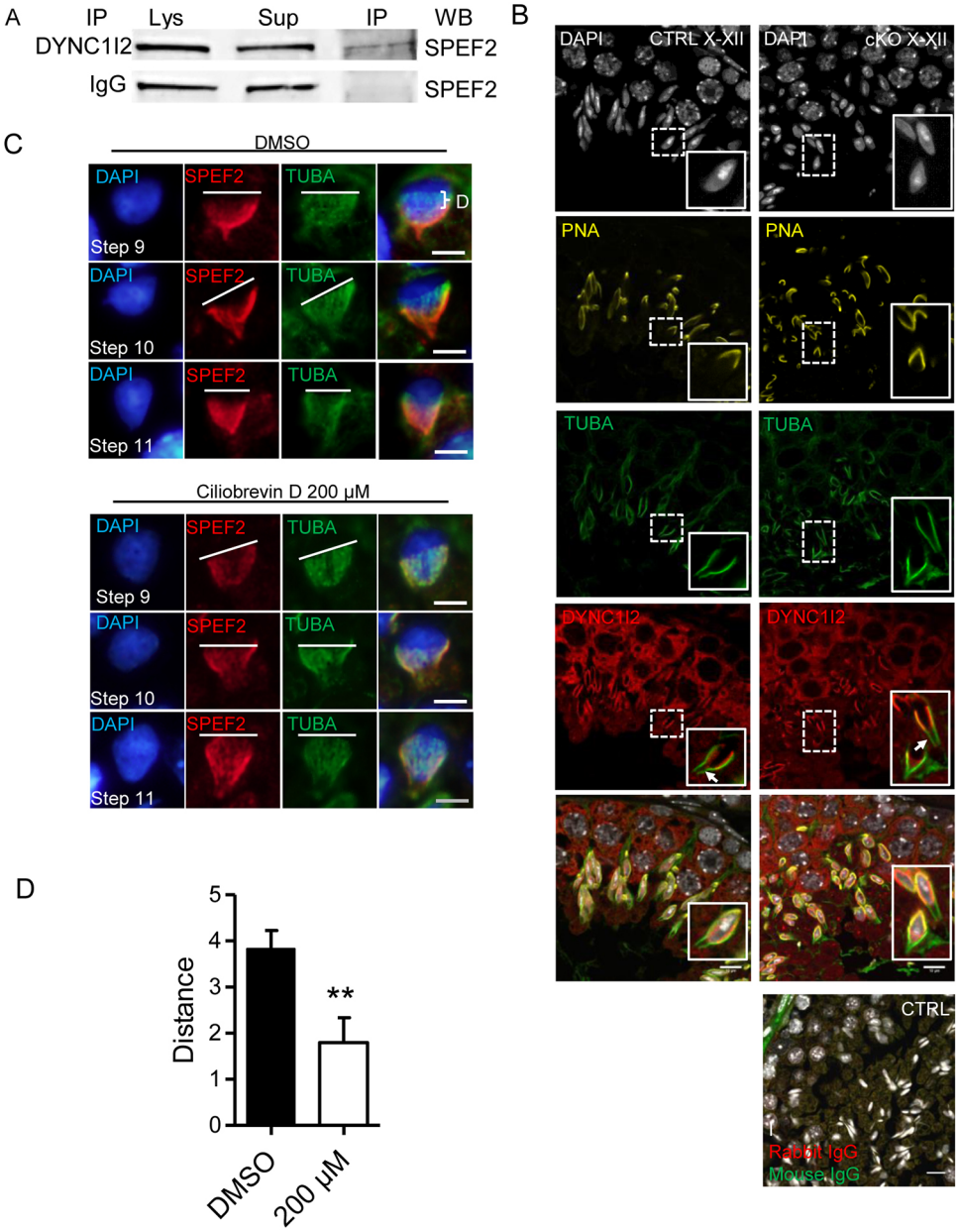

Fig. 4. Dynein 1 mobilizes SPEF2 in elongating spermatids. (A) DYNC1I2 antibody pulled down SPEF2 from CTRL testis lysates. Rabbit IgG was used as a negative control. lys, lysate; sup, supernatant collected from beads after immunoprecipitation; IP, protein eluate fraction. WB, western blot. (B) In PFA-fixed testis sections DYNC1I2 (red) localizes in the cytoplasm of spermatocytes and the manchette of elongating spermatids. DYNC1I2 localization was identical between CTRL and cKO. α-tubulin (green) stains the manchette and PNA (yellow) stains the acrosome. The manchette microtubules that are projecting over the basal body are DYNC1I2 negative (arrow). Rabbit and mouse IgG were used as negative controls. (C) Stage IX-XI segments were cut from seminiferous tubules of the CTRL mouse and incubated in the presence of ciliobrevin D or DMSO for 3 h. After incubation the cells were spread out from the tubule for immunofluorescence staining. In control (DMSO-treated) tubules the SPEF2 staining (red) appeared only at the more basal side below the perinuclear ring of the manchette, as compared with the α-tubulin-stained (green) microtubules. The SPEF2 staining was retained throughout the whole area of the manchette after ciliobrevin D treatment. (D) Quantification of the distance from the perinuclear ring to the beginning of the SPEF2 signal (labeled as D in panel C) after 3 h of DMSO or 200 µM ciliobrevin D treatment in step 9-11 spermatids. *n*=42 (DMSO) or *n*=22 (ciliobrevin D) step 9-11 spermatids. Error bars indicate s.e.m. $^{**}P<0.01$ (two-tailed Student's *t*-test). Scale bars: 10 µm in B; 5 µm in C.

showed that GOLGA3 localizes to the acroplaxome, which further supports its possible role in Golgi-derived vesicular transport during spermiogenesis.

The role of dynein 1 in vesicle transport from the Golgi complex to the basal body during ciliogenesis in the retina has been demonstrated previously (Kong et al., 2013). Unfortunately, we were unable to study the involvement of the dynein motor in the transport of SPEF2 from the Golgi complex in tubule culture conditions, since the Golgi was dispersed due to dynein inhibition. However, it is tempting to speculate that the dynein motor mobilizes SPEF2 from the Golgi complex as it does in the manchette. It is clear that further studies are required to clarify the possible interplay between SPEF2, GOLGA3 and dynein 1 in the vesicular transport from the Golgi complex.

In conclusion, our results confirmed that SPEF2 is required for axonemal CP assembly during spermiogenesis and, importantly, we identified a novel role for SPEF2 in manchette-mediated transport and sperm head shaping. Furthermore, our results suggest that SPEF2 is involved in Golgi-associated transport in male germ cells. Altogether, these results underline the importance of SPEF2 and IFT-related proteins outside the cilium, and suggest that the crucial role of SPEF2 in spermatogenesis and male fertility derives from its involvement in a broad range of transport processes during male germ cell differentiation.

MATERIALS AND METHODS

Generation of the *Spef2* targeting vector

To generate the cKO mouse model, a *Spef2* bacterial artificial clone (BAC; RP23-340E4) containing exons 3-5 (including 3′ and 5′ flanking regions) of the mouse *Spef2* gene (chromosome 15) was purchased from the Children's Hospital Oakland Research Institute (Oakland, CA, USA). A DNA fragment carrying ampicillin resistance and 50 bp homology arms for the *Spef2* gene was amplified from plasmid pACYC177 (New England Biolabs) using antisense primer 5′-AACAGAAGTATTGGAAATCTGGTTCCATGCACGTAACCACAGAGTAGTCTGGCAGACCTCAGCGCTAG-3′ and sense primer 5′-ATTCTGCTGATCCACGAGTATGGGAGTTCCTTTGTGTGGGCTATTTCATTTGAAGACGAAAGGGCCTC-3′, and electroporated into electrocompetent *E. coli* cells containing the BAC clone to generate a

Development (2017) 144, 2683-2693 doi:10.1242/dev.152108

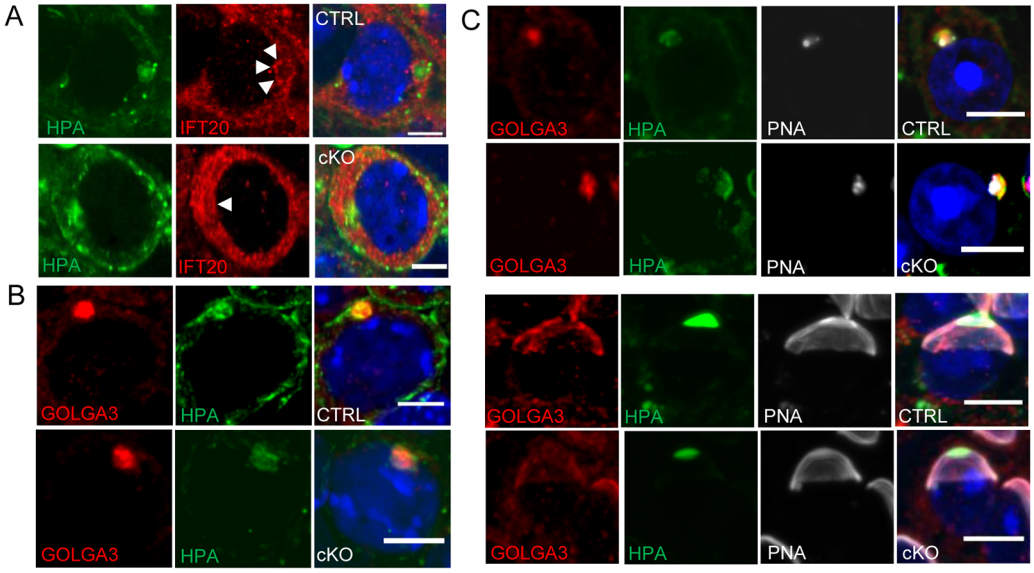

Fig. 5. The effect of *Spef2* depletion on IFT20 and GOLGA3 localization in the Golgi complex during spermatogenesis. (A) IFT20-specific (red) ring-shaped signal (arrowheads) was detected in the Golgi complex (HPA, green) of spermatocytes in CTRL mice in PFA-fixed testis sections, but in cKO the IFT20 staining was more cytoplasmic. (B) GOLGA3 (red) localizes in the Golgi complex in spermatocytes. (C) GOLGA3 localizes in the Golgi complex and the acrosome/acroplaxome in round spermatids. The GOLGA3 localization appeared similar in CTRL and cKO mice. HPA (green) stains the Golgi complex and DAPI (blue) the nuclei. Scale bars: 10 µm.

plasmid containing the *Spef2* DNA fragment by Red/ET recombination according to the manufacturer's instructions (Gene Bridges). To insert a single loxP site, a floxed PGK-Neo cassette (Gene Bridges) containing 50 bp *Spef2* homology arms was amplified by PCR using antisense primer 5′-TGGTCTAGTAAACTATATCTCCAGTGCATGTATTTTAATTTAAAATGTTTGGCGGATTTGTCCTACTCAGG-3′ and sense primer 5′-AATGTGGCTT-

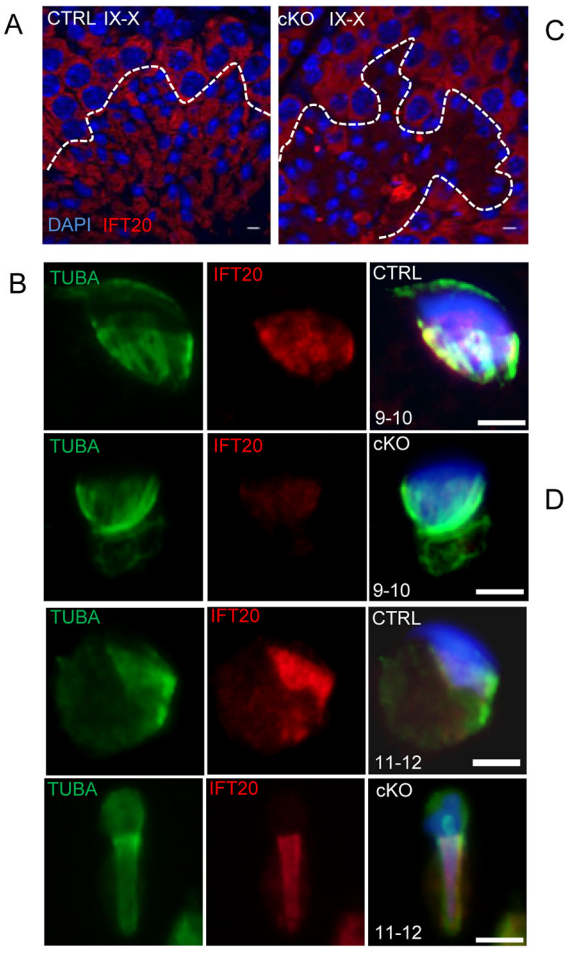

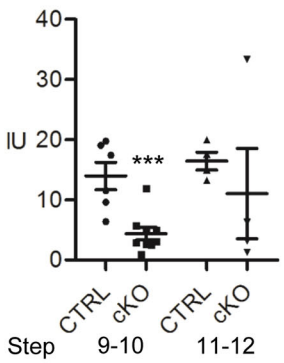

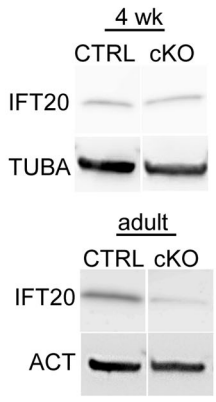

Fig. 6. IFT20 localization is affected during spermatogenesis in cKO mice. (A) IFT20-specific signal (red) was greatly reduced in the cytoplasm of cKO elongating spermatids at stages IX-X. DAPI (blue) stains the nuclei. The elongating spermatids are delineated. (B) In stage-specific drying-down preparations, IFT20 (red) appearance in the manchette was delayed in cKO spermatids. α-tubulin (green) stains the manchette and DAPI (blue) stains nuclei. (C) IFT20 signal intensity was quantified in the manchette of step 9-12 spermatids. The IFT20 signal was reduced and appeared later in the manchette of cKO mice. CTRL, *n*=6 step 9-10 and *n*=4 step 11-12; cKO, *n*=9 step 9-10 and *n*=4 step 11-12. Error bars indicate s.e.m. ***P<0.001 (two-tailed Student's *t*-test). (D) Western blot analysis to show IFT20 protein levels in 4-week-old and adult CTRL and cKO mice testis lysates. α-tubulin (TUBA) and β-actin (ACT) were used as loading controls. Scale bars: 10 µm.

Development (2017) 144, 2683-2693 doi:10.1242/dev.152108

CTTATAAATCCCAGAAATGTTAATTGGCTTGTTGCTGTTAGAAG-CAGGGATTCTGCAAAC-3′ and inserted into intron 5 by the Red/ET recombination method. In order to leave a single loxP site, site-specific recombination was carried out *in vitro* using Cre recombinase in *E.coli* (New England Biolabs). Finally, a DNA fragment containing loxP, Frt and DsRed2 was amplified from plasmid pIRES2-DsRed2 using antisense primer 5′-CTAATATCTTAAGTTAATCCTAAATTTTAACTTGACAAT-AGTTCTTTCATATAACTTCGTATAATGTATGCTATACGAAGTTATA-AGCTTGAAGTTCCTATACTTTCTAGAGAATAGGAACTTCGGATT-TTGGTCATGA*ATAACTTCGTATAATGTATGCTATACGAAGTTAT*AAGC-TTgaagttcctatactttctagagaataggaacttc*ggattttggtcatgagattat*-3′ and sense primer 5′-AGAATGATTCCCATAGCTAACATGA-TTCAGTTAAATA-ATGTTGAGAGTTTgaagttcctattctctagaaagtataggaacttc**CCAGCTAACC-AGTAACCTCTGCCCTTTCTCCTCCATGACAACCAG**gtcccgaaaac-caaagaagaagaGCCACC*atggcctcctccgagaacgt*-3′ and inserted into intron 2 by Red/ET recombination. In primer sequences the homology arms are in capital letters and underlined, loxP site is in capital italic letters, Frt site is in lowercase letters, DsRed is in lowercase and italics, En2_exon2 is in underlined lowercase letters and En2_intron1 is in capital bold letters. The validity of the targeting construct was confirmed by restriction enzyme digestion and sequencing. The *Spef2* targeting vector was linearized using *Sac*II (Promega) before targeting.

Generation of *Spef2* cKO mice (*Mus musculus*)

Linearized *Spef2* targeting vector was electroporated into hybrid mouse embryonic stem cells (ESCs; G4, 129S6B6F1) and homologous recombination in ESCs was screened by long-range (LR)-PCR and confirmed by sequencing. To generate chimeric mice, ESCs were injected into mouse C57BL/N6 blastocysts and chimera were genotyped from DNA samples isolated from ear marks by PCR. Primers for *Spef2* genotyping PCR were antisense 5′-TAACAGCCCATATCTTGAGTGATG-3′ (upstream from the loxP site after exon 5) and sense 5′-TAGCAGGATGTAGCTT-GAGCCC-3′ (downstream from exon 5). Chimeric mice were bred with C57BL/N6 wild-type mice to test germline transmission. Three chimeric male mice were born and two of them went to germline. One founder was bred with a C57BL/6-Tg(CAG-Flpe)2Arte (TaconicArtemis) mouse to remove the reporter gene, DsRed2 and stop codon before the loxP site and exon 3 by FLP-FRT recombination to produce floxed mice containing two loxP sites surrounding exons 3-5 ($Spef2^{fl/fl}$). $Spef2^{fl/fl}$ mice were further bred with Cre-expressing mice to generate the male germ cell-specific cKO mouse model. Cre was expressed under the neurogenin 3 (*Ngn3*) promoter, the expression of which begins at postnatal day 5 (Korhonen et al., 2011; Lehti et al., 2013). Mice were earmarked and DNA was isolated for genotyping by PCR. Primers used for *Spef2* genotyping were sense 5′-GATTCTTAAATTTTGAGGCC-3′ and antisense 5′-ATGCTGTTCAGT-GGATAAAA-3′, covering a loxP site in the $Spef2^{fl}$ mice (Fig. 1A).

Animals

For all experiments, the genotype of *Spef2* cKO mice was $Spef2^{fl/-};Cre^{+}$. We used two different genotypes as control (CTRL) mice: for immunofluorescence, electron microscopy and histology we used $Spef2^{fl/-}$ without Cre expression ($Spef2^{fl/-}$); and for immunoprecipitation, western blot and seminiferous tubule cultures we used wild-type C57BL/6N mice. The phenotype of $Spef2^{fl/-}$ mice was identical to that of C57BL/6N wild-type mice. All mice presented normal health status. Mice were maintained under specific pathogen-free conditions in the Central Animal Laboratory at the University of Turku. Mice were sacrificed with CO_2 and cervical dislocation. Mice were handled in accordance with international guidelines on the care and use of laboratory animals. All animal studies were approved by the Finnish Ethical Committee for Experimental Animals (licence 315/041003/2011 and 2009-1206-Kotaja).

RT-PCR

Testis from CTRL and cKO mice were dissected, snap frozen in liquid nitrogen and stored at −80°C. Total RNA was extracted using the RNeasy Midi Kit (Qiagen) and reverse transcribed using an RT-PCR Kit (Promega) following the manufacturer's instructions. *Spef2*-specific primers (*Spef2* exon 1 forward 5′-CTGGAAAGTTCCTAGCACCTGCAAG-3′, *Spef2* exon 3 reverse 5′-GTTTGGTTGCTGCCCCAGGCTT-3′, *Spef2* exon 9 reverse 5′-GCACGGTGATCCTCAGTGGG-3′) were used for PCR and the products were visualized on an agarose gel.

Co-immunoprecipitation (co-IP) and western blot

Testes from 4-week-old CTRL and cKO mice were dissected and frozen in liquid nitrogen. The four-week time point was selected to maximize the number of manchette-containing elongating spermatids in the lysate (at this time point, the first wave of spermatogenesis has reached the spermatid elongation phase). For protein extraction the testis was placed in non-denaturing lysis buffer [50 mM Tris-HCl pH 8.0, 170 mM NaCl, 1% Triton X-100, 5 mM EDTA, 1 mM DTT, phenylmethylsulfonyl fluoride (PMSF) and protease inhibitor (Complete Mini, Roche Diagnostic)] and homogenized using an UltraTurrax homogenizor. The testis lysate was incubated on ice for 20 min and centrifuged at 13,000 rpm (14,000 ***g***) for 20 min at 4°C. For western blot analysis 100 µg total protein was loaded onto 4-20% Mini-PROTEAN TGX precast gels or stain-free gels (Bio-Rad) and the gel run at 90 V for 2 h, then transferred to Hybond (GE Healthcare) membrane activated in methanol before electroblotting. Following transfer the membrane was first blocked with 5% non-fat milk in PBS containing Triton X-100 (PBST) at 0.1% for 1 h at room temperature. Anti-SPEF2 antibody KPL2end (1:300) (Sironen et al., 2010), anti-IFT20 antibody (1:100, Abnova, H00090410-B01P), anti-α-tubulin (1:1000, NeoMarkers, MS-581-P) and β-actin (1:1000, Sigma Aldrich, A5441) were diluted in 1% non-fat milk in 0.1% PBST and incubated overnight at 4°C. After washes, membranes were incubated with secondary antibodies (1:3000, HRP-conjugated anti-rabbit IgG, GE Healthcare Life Sciences) for 1 h at room temperature. Bound antibodies were visualized with ECL Plus western blotting detection system (Amersham Pharmacia) and LAS4000 luminescence imager (Fujifilm). Co-IP was performed using Protein G Dynabeads according to the manufacturer's protocol (1003D, Thermo Fischer Scientific). Antibodies used for co-IP were KPL2end and DYNC1I2 (ProteinTech, 12219-1-AP) (Inaba et al., 2016). Antibody qualification data are presented in Fig. S1A,B. For mass spectrometry, immunoprecipitated proteins were run on a gel, and the specific regions of the gel (Fig. S1C) were cut out and subjected to in-gel digestion.

Paraffin-embedded testis sections

The testis and epididymis were dissected from adult CTRL and cKO mice and fixed with 4% paraformaldehyde (PFA) or Bouin fixative overnight before paraffin embedding. Testis or epididymis blocks were cut and stained with periodic acid-Schiff (PAS) or Hematoxylin and Eosin (HE), respectively. For immunofluorescence the paraffin was removed with xylene and sections were dehydrated in a decreasing alcohol series. Slides were treated with 10 mM sodium citrate buffer (pH 6.0), 0.05% Tween 20 in a pressure cooker. Non-specific antibody binding sites were blocked with blocking solution (10% normal donkey serum, 3% BSA in 0.01% PBST) for 1 h at room temperature. Primary antibodies were diluted in 3% normal donkey serum, 1% BSA in 0.01% PBST and incubated overnight at 4°C. Primary antibodies were against acetylated-tubulin (1:1500, Sigma, T7451, clone 6-11B-1), α-tubulin (1:1000, NeoMarkers, MS-581-P), DYNC1I2 (1:600, Proteintech), IFT20 (1:200) (Pazour et al., 2002), γ-tubulin (1:1000, Abcam, ab11316), mouse IgG (1:1000, Santa-Cruz, sc-2025), rabbit IgG (1:1000, NeoMarkers, NC-100-P1) and GOLGA3A (1:1000) (Chandran and Machamer, 2008). After washes the slides were incubated with secondary antibodies (anti-mouse/rabbit Alexa Fluor 488/594, 1:500, Molecular Probes) for 1 h at room temperature. Peanut agglutinin (PNA, Vector Laboratories, RL-1072) was diluted 1:15,000 to visualize the acrosome, and *Helix pomatia* lectin (HPA, Life Technologies, L11271) was diluted 1:250 to visualize the Golgi complex, and then incubated together with secondary antibodies. Nuclei were visualized with DAPI (Sigma-Aldrich, D9542) and slides were mounted with Prolong Diamond Antifade Mountant (Life Technologies, P36970). Slides were visualized using a 3i spinning disk confocal microscope (Intelligent Imaging Innovations) and figures were prepared with Fiji (Schindelin et al., 2012).

Drying-down preparations

Testes from CTRL and cKO mice were collected in PBS. Drying-down preparations from stage-specific segments of seminiferous tubules were

Development (2017) 144, 2683-2693 doi:10.1242/dev.152108

prepared according to the protocol of Kotaja et al. (2004). For immunofluorescence, cells were fixed with 4% PFA, treated with 100 mM ammonium chloride to quench autofluorescence and permeabilized with 0.2% PBST. Slides were blocked with blocking solution and primary antibodies to α-tubulin (1:1000) and IFT20 (1:200) were incubated overnight at 4°C. After washes, secondary antibodies were added (anti-mouse/rabbit Alexa Fluor 488/594, 1:500) for 1 h at room temperature. Nuclei were visualized with DAPI. Slides were mounted with Prolong Diamond Antifade Mountant and visualized using a Leica DMRBE microscope. IFT20 intensity was measured from the manchette with Fiji.

Electron microscopy

Stage-specific pieces of seminiferous tubule were cut and fixed in 5% glutaraldehyde and treated with potassium ferrocyanide-osmium fixative. Tubules were embedded in epoxy resin and stained with 1% uranyl acetate and 0.3% lead citrate. Preparations were visualized with a JEM-1400 Plus (JEOL) electron microscope.

Seminiferous tubule culture and squash immunofluorescence

Stage IX-XI seminiferous tubules were dissected from the CTRL mouse testis. Tubules were placed in a 96-well plate and incubated in DMEM with dimethylsulfoxide (DMSO) or 200 µM ciliobrevin D (Merck Millipore, 250401). After 3 h incubation, tubules were placed on a microscope slide. A coverslip was placed on top and cells were spread out from the tubules. Slides were snap frozen in liquid nitrogen to remove the coverslip, and cells were fixed in acetone for 10 min and air dried overnight at room temperature. Slides were stored at −80°C or used immediately for immunofluorescence. Slides were postfixed in 4% PFA, and treated with 0.2% PBST before blocking in 10% normal donkey serum in 0.1% PBST. Primary antibodies were against α-tubulin (1:1000) and SPEF2 (1:200, Sigma Aldrich, HPA039606). After overnight incubation at 4°C the slides were washed with PBS and then incubated with secondary antibodies for 1 h at room temperature. All antibodies were diluted in 3% normal donkey serum in 0.1% PBST. Nuclei were visualized using DAPI and slides were mounted with Prolong Diamond Antifade Mountant. Dynein inhibitory effect was analyzed by measuring the distance between SPEF2 and α-tubulin within the manchette from the perinuclear ring using PhotoShop CS4 (Adobe).

Statistical analysis

Data are presented as average values with s.e.m. Statistical analysis was performed using Student's *t*-test and $P<0.05$ was considered statistically significant.

Acknowledgements

We are grateful to Professor Carolyn Machamer (School of Medicine, Department of Cell Biology, Baltimore, MD, USA) for GOLGA3A antibody and Professor G. J. Pazour (University of Massachusetts Medical School, Worcester, MA, USA) for IFT20 antibody. We thank the Turku Center for Disease Modeling, and the Central Animal Laboratory of the University of Turku for generating *Spef2* cKO mice and the housing of the animals. The Turku Center for Biotechnology Imaging Core Facility and the Electron Microscopy Unit at the University of Turku are acknowledged. Mass spectrometry analysis was performed at the Turku Proteomics Facility, University of Turku and Åbo Akademi University, which is supported by Biocenter Finland. The help of laboratory technicians Tarja Hovivuori, Johanna Rusi, Anneli Virta and Jonna Tabell of the Natural Resources Institute Finland (Luke) in genotyping and gene expression analysis is greatly appreciated.

Competing interests

The authors declare no competing or financial interests.

Author contributions

Methodology: M.S.L., F.-P.Z., N.K., A.S.; Validation: M.S.L., F.-P.Z., N.K., A.S.; Formal analysis: M.S.L., F.-P.Z., N.K., A.S.; Investigation: M.S.L., N.K., A.S.; Resources: N.K., A.S.; Writing - original draft: M.S.L., A.S.; Writing - review & editing: M.S.L., F.-P.Z., N.K., A.S.; Visualization: M.S.L., N.K., A.S.; Supervision: N.K., A.S.; Project administration: N.K., A.S.; Funding acquisition: M.S.L., N.K., A.S.

Funding

This work was funded by the Turku Doctoral Programme of Molecular Medicine (TuDMM) of the University of Turku (Turun Yliopisto) (M.S.L.); Finnish Cultural Foundation's Häme Regional Fund (Hämeen Rahasto) (M.S.L.); Finnish Cultural Foundation's Varsinais-Suomi Regional Fund (Varsinais-Suomen Rahasto) (M.S.L.); Academy of Finland (Suomen Akatemia) (N.K., M.S.L., A.S.); and Sigrid Jusélius Foundation (Sigrid Juséliuksen Säätiö) (N.K.).

Supplementary information

Supplementary information available online at
http://dev.biologists.org/lookup/doi/10.1242/dev.152108.supplemental

References

Bentson, L. F., Agbor, V. A., Agbor, L. N., Lopez, A. C., Nfonsam, L. E., Bornstein, S. S., Handel, M. A. and Linder, C. C. (2013). New point mutation in Golga3 causes multiple defects in spermatogenesis. *Andrology* **1**, 440-450.

Chandran, S. and Machamer, C. E. (2008). Acute perturbations in golgi organization impact de novo sphingomyelin synthesis. *Traffic* **9**, 1894-1904.

Firestone, A. J., Weinger, J. S., Maldonado, M., Barlan, K., Langston, L. D., O'Donnell, M., Gelfand, V. I., Kapoor, T. M. and Chen, J. K. (2012). Small-molecule inhibitors of the AAA+ ATPase motor cytoplasmic dynein. *Nature* **484**, 125-129.

Follit, J. A., Tuft, R. A., Fogarty, K. E. and Pazour, G. J. (2006). The intraflagellar transport protein IFT20 is associated with the golgi complex and is required for cilia assembly. *Mol. Biol. Cell* **17**, 3781-3792.

Hayasaka, S., Terada, Y., Suzuki, K., Murakawa, H., Tachibana, I., Sankai, T., Murakami, T., Yaegashi, N. and Okamura, K. (2008). Intramanchette transport during primate spermiogenesis: expression of dynein, myosin Va, motor recruiter myosin Va, VIIa-Rab27a/b interacting protein, and Rab27b in the manchette during human and monkey spermiogenesis. *Asian J. Androl.* **10**, 561-568.

Hu, W. F., Pomp, O., Ben-Omran, T., Kodani, A., Henke, K., Mochida, G. H., Yu, T. W., Woodworth, M. B., Bonnard, C., Raj, G. S. et al. (2014). Katanin p80 regulates human cortical development by limiting centriole and cilia number. *Neuron* **84**, 1240-1257.

Inaba, H., Goto, H., Kasahara, K., Kumamoto, K., Yonemura, S., Inoko, A., Yamano, S., Wanibuchi, H., He, D., Goshima, N. et al. (2016). Ndel1 suppresses ciliogenesis in proliferating cells by regulating the trichoplein-aurora A pathway. *J. Cell Biol.* **212**, 409-423.

Jin, M., Pomp, O., Shinoda, T., Toba, S., Torisawa, T., Furuta, K., Oiwa, K., Yasunaga, T., Kitagawa, D., Matsumura, S. et al. (2017). Katanin p80, NuMA and cytoplasmic dynein cooperate to control microtubule dynamics. *Sci. Rep.* **7**, 39902.

Kierszenbaum, A. L., Rivkin, E. and Tres, L. L. (2011a). Cytoskeletal track selection during cargo transport in spermatids is relevant to male fertility. *Spermatogenesis* **1**, 221-230.

Kierszenbaum, A. L., Rivkin, E., Tres, L. L., Yoder, B. K., Haycraft, C. J., Bornens, M. and Rios, R. M. (2011b). GMAP210 and IFT88 are present in the spermatid golgi apparatus and participate in the development of the acrosome-acroplaxome complex, head-tail coupling apparatus and tail. *Dev. Dyn.* **240**, 723-736.

Kong, S., Du, X., Peng, C., Wu, Y., Li, H., Jin, X., Hou, L., Deng, K., Xu, T. and Tao, W. (2013). Dlic1 deficiency impairs ciliogenesis of photoreceptors by destabilizing dynein. *Cell Res.* **23**, 835-850.

Korhonen, H. M., Meikar, O., Yadav, R. P., Papaioannou, M. D., Romero, Y., Da Ros, M., Herrera, P. L., Toppari, J., Nef, S. and Kotaja, N. (2011). Dicer is required for haploid male germ cell differentiation in mice. *PLoS ONE* **6**, e24821.

Kotaja, N., Kimmins, S., Brancorsini, S., Hentsch, D., Vonesch, J.-L., Davidson, I., Parvinen, M. and Sassone-Corsi, P. (2004). Preparation, isolation and characterization of stage-specific spermatogenic cells for cellular and molecular analysis. *Nat. Methods* **1**, 249-254.

Lehti, M. S., Kotaja, N. and Sironen, A. (2013). KIF3A is essential for sperm tail formation and manchette function. *Mol. Cell. Endocrinol.* **377**, 44-55.

Navolanic, P. M. and Sperry, A. O. (2000). Identification of isoforms of a mitotic motor in mammalian spermatogenesis. *Biol. Reprod.* **62**, 1360-1369.

Nigg, E. A. and Stearns, T. (2011). The centrosome cycle: centriole biogenesis, duplication and inherent asymmetries. *Nat. Cell Biol.* **13**, 1154-1160.

Nozawa, Y. I., Yao, E., Gacayan, R., Xu, S.-M. and Chuang, P.-T. (2014). Mammalian fused is essential for sperm head shaping and periaxonemal structure formation during spermatogenesis. *Dev. Biol.* **388**, 170-180.

O'Donnell, L., Rhodes, D., Smith, S. J., Merriner, D. J., Clark, B. J., Borg, C., Whittle, B., O'Connor, A. E., Smith, L. B., McNally, F. J. et al. (2012). An essential role for Katanin p80 and microtubule severing in male gamete production. *PLoS Genet.* **8**, e1002698.

Ostrowski, L. E., Andrews, K., Potdar, P., Matsuura, H., Jetten, A. and Nettesheim, P. (1999). Cloning and characterization of KPL2, a novel gene induced during ciliogenesis of tracheal epithelial cells. *Am. J. Respir. Cell Mol. Biol.* **20**, 675-683.

Pazour, G. J., Baker, S. A., Deane, J. A., Cole, D. G., Dickert, B. L., Rosenbaum, J. L., Witman, G. B. and Besharse, J. C. (2002). The intraflagellar transport protein, IFT88, is essential for vertebrate photoreceptor assembly and maintenance. *J. Cell Biol.* **157**, 103-114.

Saade, M., Irla, M., Govin, J., Victorero, G., Samson, M. and Nguyen, C. (2007). Dynamic distribution of spatial during mouse spermatogenesis and its interaction with the kinesin KIF17b. *Exp. Cell Res.* **313**, 614-626.

Schindelin, J., Arganda-Carreras, I., Frise, E., Kaynig, V., Longair, M., Pietzsch, T., Preibisch, S., Rueden, C., Saalfeld, S., Schmid, B. et al.

Development (2017) 144, 2683-2693 doi:10.1242/dev.152108

(2012). Fiji: an open-source platform for biological-image analysis. *Nat. Methods* **9**, 676-682.

Scholey, J. M. (2013). Cilium assembly: delivery of tubulin by Kinesin-2-powered trains. *Curr. Biol.* **23**, R956-R959.

Schvarzstein, M., Pattabiraman, D., Bembenek, J. N. and Villeneuve, A. M. (2013). Meiotic HORMA domain proteins prevent untimely centriole disengagement during Caenorhabditis elegans spermatocyte meiosis. *Proc. Natl. Acad. Sci. USA* **110**, E898-E907.

Sironen, A. I., Andersson, M., Uimari, P. and Vilkki, J. (2002). Mapping of an immotile short tail sperm defect in the Finnish Yorkshire on porcine chromosome 16. *Mamm. Genome* **13**, 45-49.

Sironen, A., Thomsen, B., Andersson, M., Ahola, V. and Vilkki, J. (2006). An intronic insertion in KPL2 results in aberrant splicing and causes the immotile short-tail sperm defect in the pig. *Proc. Natl. Acad. Sci. USA* **103**, 5006-5011.

Sironen, A., Hansen, J., Thomsen, B., Andersson, M., Vilkki, J., Toppari, J. and Kotaja, N. (2010). Expression of SPEF2 during mouse spermatogenesis and identification of IFT20 as an interacting protein. *Biol. Reprod.* **82**, 580-590.

Sironen, A., Kotaja, N., Mulhern, H., Wyatt, T. A., Sisson, J. H., Pavlik, J. A., Miiluniemi, M., Fleming, M. D. and Lee, L. (2011). Loss of SPEF2 function in mice results in spermatogenesis defects and primary ciliary dyskinesia. *Biol. Reprod.* **85**, 690-701.

Taschner, M. and Lorentzen, E. (2016). The intraflagellar transport machinery. *Cold Spring Harb. Perspect. Biol.* **8**, a028092.

Ververis, A., Christodoulou, A., Christoforou, M., Kamilari, C., Lederer, C. W. and Santama, N. (2016). A novel family of Katanin-Like 2 protein isoforms (KATNAL2), interacting with nucleotide-binding proteins Nubp1 and Nubp2, are key regulators of different MT-based processes in mammalian cells. *Cell. Mol. Life Sci.* **73**, 163-184.

Yadav, S., Puthenveedu, M. A. and Linstedt, A. D. (2012). Golgin160 recruits the dynein motor to position the golgi apparatus. *Dev. Cell* **23**, 153-165.

Yoshida, T., Ioshii, S. O., Imanaka-Yoshida, K. and Izutsu, K. (1994). Association of cytoplasmic dynein with manchette microtubules and spermatid nuclear envelope during spermiogenesis in rats. *J. Cell Sci.* **107**, 625-633.